Contribution from the Rockwell International Science Center, Thousand Oaks, California 91360, and Rocketdyne, A Division of Rockwell International, Canoga Park, California 91304

Electron Spin Resonance Spectra of the $^{14}NF_3^{+}\cdot$ and $^{15}NF_3^{+}\cdot$ Radical Cations

I. B. GOLDBERG,* H. R. CROWE, and K. O. CHRISTE

Received April 18, 1978

The ESR spectra of the $^{14}NF_3^{+}\cdot$ and $^{15}NF_3^{+}\cdot$ radical cations were observed over the temperature range 15–340 K. The radical cations were generated either by γ irradiation of NF_4^+ salts or by low-temperature UV photolysis of NF_3–F_2–Lewis acid mixtures. For $NF_3^{+}\cdot$, two different types of spectra were observed. At the lower temperatures, a highly anisotropic spectrum was obtained which is attributed to a rigid radical. At the higher temperatures, a more isotropic spectrum was observed which is attributed to $NF_3^{+}\cdot$ of axial symmetry. An analysis of the observed spectra was carried out and was supported by computer simulations and the observed ^{15}N isotopic data. It was found that the previously reported value of the isotropic fluorine hyperfine splitting is incorrect. The resulting spin density distributions indicate that $NF_3^{+}\cdot$ is pyramidal but that within the isoelectronic series $BF_3^{-}\cdot$, $CF_3\cdot$, $NF_3^{+}\cdot$ the planarity of the radicals increases from $BF_3^{-}\cdot$ toward $NF_3^{+}\cdot$.

Introduction

Radicals and radical ions formed from first-row elements have been the subject of numerous studies. These species provide experimental data by which molecular orbital models can be tested and also define limits within which the properties of isoelectronic species can be predicted. Electron spin resonance (ESR) provides a useful technique for studying the structure of these radicals[1] since the spin distribution in s and p orbitals can be determined from hyperfine splittings (hfs) and limits can often be set on the energies of excited states through the g factors.[1,2]

This study was prompted by the following observations: (i) During a recent study[3] of the synthesis of NF_4^+ salts, ESR spectra were obtained which were substantially different from those previously reported.[4] The radicals exhibiting these spectra were stable up to 250 K, depending upon the particular anion. The ESR spectra recorded at these higher temperatures could not be reconciled with the parameters previously given by Mishra et al.[4] (ii) On the basis of the known isotropic fluorine hyperfine splittings (a_F(iso)) of isoelectronic $BF_3^{-}\cdot$ (17.8 mT)[5] and CF_3 (14.35 mT),[6-10] the value of 16.7 mT previously reported[4] of $NF_3^{+}\cdot$ appeared to be much too high if a monotonic trend in the values for a_F(iso) is assumed for the isoelectronic series. Since the values of the hyperfine splittings can be used to determine the structure of these radicals, a reexamination of the previously given[4] analysis of the ESR spectra seemed necessary. For this purpose, it was also found necessary to study the isotopically labeled $^{15}NF_3^{+}\cdot$ to permit unambiguous assignment of the nitrogen hfs.

In this paper we report the ESR spectra of $^{14}NF_3^{+}\cdot$ and $^{15}NF_3^{+}\cdot$, including a study of their temperature dependencies and a revised analysis of the hyperfine splittings.

Experimental Section

Synthesis of $^{15}NF_4^+$ Salts. The low-temperature UV photolysis experiments of NF_3–F_2–Lewis acid mixtures were carried out in quartz containers as previously described.[3] The $^{15}NF_3$ used in some of these experiments was prepared by glow discharge of $^{15}N_2$ (99% ^{15}N, Stohler Isotope Chemicals) and F_2 (Rocketdyne) mixtures according to the method of Maya.[11] The samples of NF_4BF_4 and NF_4AsF_6 used for the ^{60}Co γ-irradiation experiments were prepared by low-temperature UV photolysis in a quartz reactor using a previously described[12] method. The samples of NF_4^+ antimonates were prepared by heating mixtures of NF_3, F_2, and SbF_5 at elevated pressures in a Monel cylinder.[13] These salts were recrystallized from anhydrous HF to remove residual Monel salt impurities.

γ Irradiation. NF_4^+ salts were transferred in a dry nitrogen atmosphere into 4-mm o.d. quartz tubes (J. F. Scanlon Co., Solvang, Calif.) which were flame-sealed under vacuum. Typically, samples of 100 mg of $^{14}NF_4^+$ salts were used while only 15-mg samples of $^{15}NF_4^+$ salts were available. Samples were exposed to ^{60}Co γ irradiation at 77 K, using a flux rate of 4×10^5 R h^{-1}. Samples of the $^{14}NF_4^+$ salts were exposed between 15 and 24 h, while the sample of the $^{15}NF_4^+$ salt was exposed for 40 h. Samples were annealed in dry ice (195 K) prior to recording their ESR signals. The $NF_3^{+}\cdot$ signal intensity did not decrease even when the samples were stored at 195 K for several months.

UV Experiments. The conditions used for the UV photolyses have previously been described.[3]

ESR Spectra. ESR spectra were recorded using a computer-controlled ESR spectrometer previously described.[14] The spectrometer operated at 9.303 GHz with a TE_{104} rectangular dual cavity and an LTD-3-110 (Air Products) Helitran temperature controller. A 15-in. magnet was used with the spectrometer. Signal averaging combined with programs for smoothing spectra and removal of background signals was used to record weak spectra. Intense spectra were recorded using standard dual cavity techniques. The magnetic field standard was Mn^{2+}.[15] Values of the magnetic parameters were $a_{Mn} = 8.673 \pm 0.003$ mT (1 T = 10^4 Oe) and $g = 2.000\,95 \pm 0.000\,05$.[16] Field positions were computed to third order. Spectra were recorded between 15 and 340 K.

Simulations of ESR Spectra. Simulations of the ESR spectra of powders were carried out using a program developed by White and Belford based on the method of Pilbrow and Winfield[17] and modified by Chasteen.[18] The program computes second-order shifts of one nucleus and permits the hyperfine axis of that nucleus to be nonparallel to the remainder of the hyperfine axes. It also allows anisotropic line widths to be used in the calculation. The program was further modified in our laboratory to include second-order splittings from one equivalent set of nuclei.

Results

ESR Spectra. During a recent ESR study[3] of the UV photolysis of mixtures of NF_3, F_2, and BF_3 or AsF_5, spectra similar to that shown in Figure 1a were observed at ca. 77 K. However, as shown in Figure 1 of ref 3, these spectra were very poorly resolved. These spectra, which were attributed to a immobile $NF_3^{+}\cdot$ radical cation in a matrix, are expected to exhibit unique features (singularities) which correspond to the orientation of the threefold symmetry axis of the radical along directions parallel and perpendicular to the applied magnetic field. However, only the parallel component of the spectrum is clearly identifiable.

Upon warming of the UV-photolyzed mixture, the spectra began to change. The thermal stability of the observed ESR signals strongly depended upon the Lewis acid used. For AsF_5 the ESR signal became more intense about 130 K and appeared to be more isotropic. At 180 K, the signal started to lose intensity, and it decayed rapidly at 230 K. This loss of signal intensity can be attributed to the disappearance of the condensed AsF_5 phase. However, a relatively weak residual signal remained above 230 K which can be attributed to $NF_3^{+}\cdot$ trapped in the solid NF_4AsF_6 formed during the UV photolysis. For the more volatile BF_3, the change from the anisotropic low-temperature spectrum to the more isotropic higher temperature one occurred at about 117 K. At 140 K, the

* To whom correspondence should be addressed at Rockwell International Science Center.

0020-1669/78/1317-3189$01.00/0

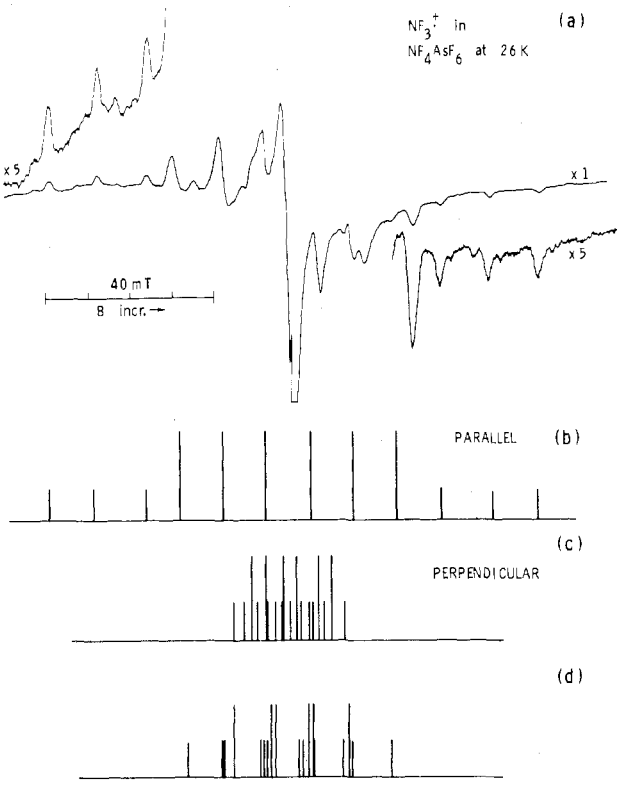

Figure 1. (a) ESR spectrum of $^{14}NF_3^{+}\cdot$ at 26 K in NF_4AsF_6 γ irradiated at 77 K after annealing at 195 K. (b) Stick plots of the line positions to first order, assuming parallel F-atom tensors with the C_{3v} axis of the radical aligned parallel to the applied field. (c) Stick plot to second order of the line positions of the radical with its C_{3v} axis perpendicular to the applied field (our analysis). (d) Stick plot to second order under conditions of (c) using the previously reported assignment. See discussion of (c) and (d) in text.

$NF_3^{+}\cdot$ signal was completely lost. Although the more isotropic spectra observed for the NF_3–F_2–AsF_5 and NF_3–F_2–BF_3 systems exhibited broad lines, it became evident that they could not be interpreted in terms of the parameters previously assigned to $NF_3^{+}\cdot$.

In order to resolve these disparities, the temperature dependence of the ESR spectra of the γ-irradiated salts of NF_4^+ was investigated. Salts used in this study were NF_4BF_4, NF_4AsF_6, NF_4SbF_6, and $NF_4SbF_6{\cdot}0.8SbF_5$, all of which gave similar spectra after γ irradiation at 77 K, followed by annealing at 195 K in solid CO_2. Contrary to Mishra,[4] no problem was encountered in generating $NF_3^{+}\cdot$ by γ irradiation of NF_4BF_4. Prior to annealing, residual signals were observed on either side of the $NF_3^{+}\cdot$ resonance, in addition to an intense sharp line at $g = 2$. The origin of these signals, which may have been due to the anion,[4] was not investigated. The annealed samples exhibited different spectra at high and low temperatures. The low-temperature spectrum, observed between 10 and 140 K, was similar to that previously attributed to $NF_3^{+}\cdot$,[4] and is shown in Figure 1 for irradiated NF_4AsF_6 at 26 K. Other salts gave similar spectra, except that the lines exhibited a shoulder to the high field side of the main resonance. The line width of the spectrum increased slightly with longer irradiation times but was independent of temperature. Reducing the amount of $NF_3^{+}\cdot$ by warming the sample resulted in a narrower line. These observations suggest that dipolar interactions occurred between nearby defect sites. There is one difference between our spectra and that observed by Mishra et al.;[4] even in the more dilute solutions, we were unable to resolve some of the features which were attributed to the alignment of the C_{3v} axis of the radical perpendicular to the magnetic field. We did, however, observe shoulders at these positions.

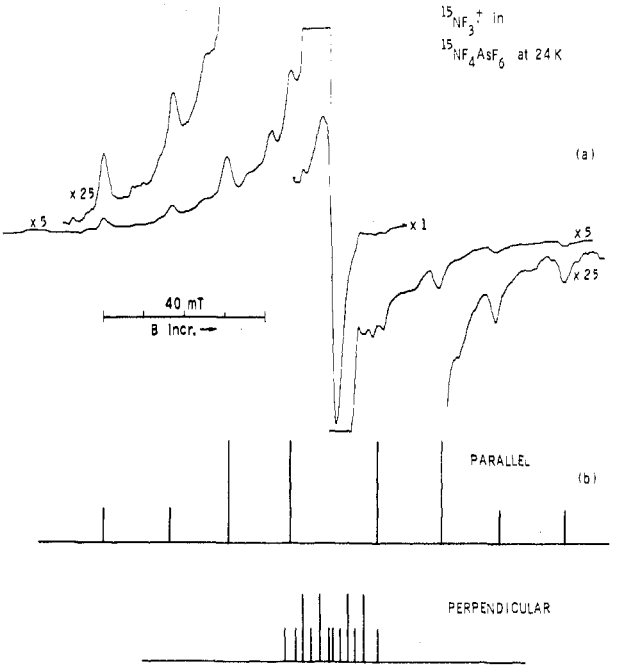

Figure 2. (a) ESR spectrum of $^{15}NF_3^{+}\cdot$ at 24 K in $^{15}NF_4AsF_6$ γ irradiated at 77 K after annealing at 195 K. (b) Stick plots of the line positions for the C_{3v} axis of the radical aligned parallel and perpendicular to the applied field, assuming parallel fluorine hfs tensors.

As the temperature of the arsenate and antimonate salts is increased to the range 140 and 235 K, the low-temperature spectrum collapses and then forms a sharper one with a narrower span. This spectrum is independent of temperature between 240 and 340 K, where decomposition begins, and is shown in Figure 3 for irradiated NF_4AsF_6 at 240 K. The lifetime of the species at room temperature is about 2 weeks but decreases to about 10 min at 340 K. Similar spectra were observed for the irradiated borate salts between about 270 and 320 K.

In order to be certain that the spectra reported here are due to $NF_3^{+}\cdot$, isotopically pure $^{15}NF_4AsF_6$ and $^{15}NF_4BF_4$ were prepared. The signal observed for the irradiated salts exhibited the same temperature dependence as those obtained for $^{14}NF_4^+$ salts. However, since only ca. 15 mg of $^{15}NF_4^+$ salts was prepared, longer irradiation times had to be used resulting in slightly broadened lines. The low-temperature spectrum of $^{15}NF_3^{+}\cdot$ in $^{15}NF_4AsF_6$ is shown in Figure 2, where the ^{14}N triplets are replaced by ^{15}N doublets. The high-temperature $^{15}NF_3^{+}\cdot$ spectrum is shown in Figure 4 and is analogous to the high-temperature $^{14}NF_3^{+}\cdot$ spectrum.

Discussion

Low-Temperature Spectra of $^{14}NF_3^{+}\cdot$. Several unusual features become apparent upon close inspection of the $NF_3^{+}\cdot$ spectra at low temperatures. Most significantly, the distinct, intense features of the spectra must be assigned to the radical with its threefold symmetry (C_{3v}) axis aligned parallel to the applied magnetic field. Generally, however, the most intense features of the spectra of axially symmetric radicals in powders are assigned to the orientation in which the symmetry axis is perpendicular to the applied field.[18-20] Since no such features are observed here, it is clear that this spectrum cannot be treated in the conventional manner used for axial or nearly axial symmetry.

A second feature is that the positions of the lines in the spectrum that correspond to the $\|$ orientation do not fall into the positions calculated from the hyperfine splittings (hfs)

Table I. Hyperfine Splittings[a] of $^{14}NF_3^+$ and $^{15}NF_3^+$ at High and Low Temperatures

	$^{14}NF_3^+$		$^{15}NF_3^+$	
	26 K	240 K	24 K	240 K
$a_F(\parallel)$	30.8[c]	2.00 ± 0.25	30.6[c]	2.40 ± 0.25
$a_F(\perp)$	(−)3.3[c]	12.48 ± 0.05	(−)3.8[c]	11.97 ± 0.05
$a_N(\parallel)$	11.49 ± 0.20	8.70 ± 0.25	−16.08 ± 0.20	−12.20 ± 0.25[c]
$a_N(\perp)$	7.8 ± 0.5	9.36 ± 0.05	−10.6 ± 1.0	−13.03 ± 0.05[c]
a_F(iso)	8.1	8.99 ± 0.14	7.7	8.78 ± 0.14
a_N(iso)	9.0	9.14 ± 0.14	−12.4	−12.75 ± 0.14
$g(\parallel)$	2.003 ± 0.002	2.0073 ± 0.0010	2.003 ± 0.002	2.0079 ± 0.0012
$g(\perp)$	2.006 ± 0.002	2.0040 ± 0.0007	2.005 ± 0.002	2.0047 ± 0.0007
g(iso)	2.005 ± 0.002	2.0051 ± 0.0007	2.005 ± 0.002	2.0058 ± 0.0009

[a] Hyperfine splittings are in mT (1 mT = 10 Oe). [b] The sign of the ^{14}N hfs is assumed to be positive; thus ^{15}N hfs are negative by virtue of their nuclear moments. [c] These are effective values based on supposed axial symmetry for individual tensors; $a_F(z) = 30.8$ mT and $a_F(x) = a_F(y) \sim 3.3$ mT (see text).

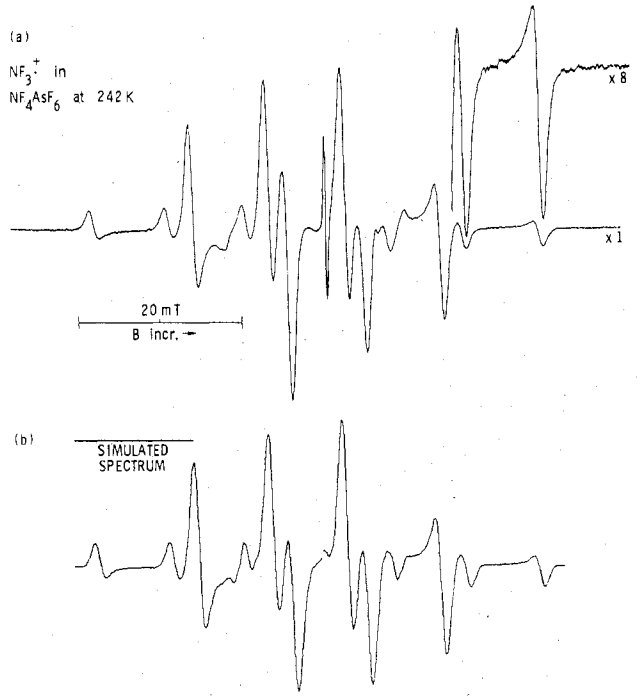

Figure 3. (a) ESR spectra of $^{14}NF_3^+$· at 242 K in NF_4AsF_6 γ irradiated at 77 K. (b) Computer simulation of spectrum assuming axial symmetry and the parameters given in Table I.

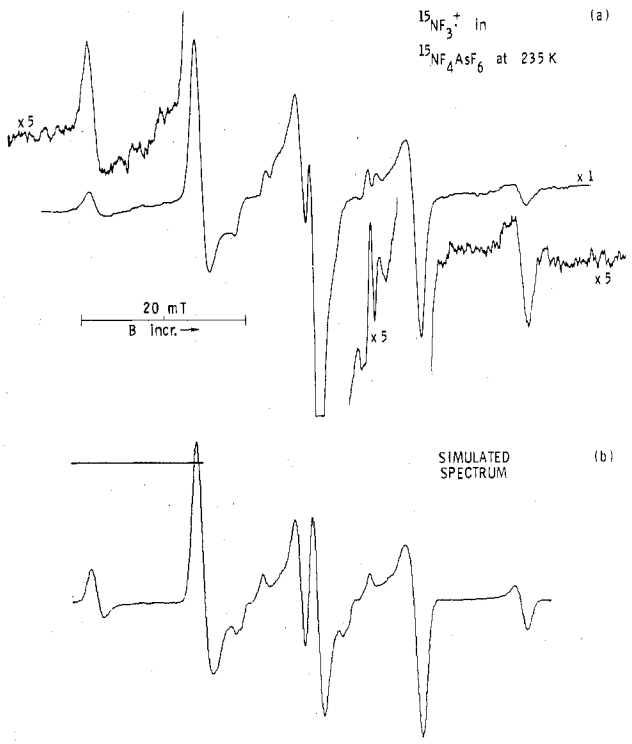

Figure 4. (a) ESR spectra of $^{15}NF_3^+$· at 235 K in $^{15}NF_4AsF_6$ γ irradiated at 77 K. (b) Computer simulation of spectrum assuming axial symmetry and parameters given in Table I.

which are given in Table I. These values are calculated from the extrema of the spectrum. For a system which exhibits a large hfs with axial symmetry, the field positions in which the unique axis is parallel to the magnetic field, $H_{I,M}(\parallel)$, is given by eq 1 to second order,[21] where $g(\parallel)$, $g(\perp)$, $a(\parallel)$, and $a(\perp)$

$$H_{I,M_I}(\parallel) = H_0(\parallel) - a(\parallel)M_I - \frac{a(\perp)^2[g(\perp)/g(\parallel)]^2}{2[H_0(\parallel) - a(\parallel)M_I]}[I(I+1) - M_I^2] \quad (1)$$

are the parallel and perpendicular g factors and hfs, respectively, $H_0(\parallel)$ is given by $h\nu/g(\parallel)\mu_B$, I is the total nuclear spin, and M_I is the component of spin parallel to the magnetic field. The analogous equation for $H_{I,M}(\perp)$ is given by eq 2,[21]

$$H_{I,M_I}(\perp) = H_0(\perp) - a(\perp)M_I - \frac{a(\perp)^2 + a(\parallel)^2[g(\parallel)/g(\perp)]^2}{4[H_0(\perp) - a(\perp)M_I]}[I(I+1) - M_I^2] \quad (2)$$

where $H_0(\perp)$ is given by $h\nu/g(\perp)\mu_B$. Field positions are plotted on the same field axis under the spectrum in Figure 1b, for the molecule oriented $\parallel$ and $\perp$ to the field. Second-order shifts are only significant for NF_3^+· when the field is $\perp$ to the C_{3v} axis of the radical. Note that for the $\parallel$ orientation, while the lines corresponding to $M_I(F) = +^3/_2$ and $-^3/_2$ agree with the calculated positions, the lines corresponding to $M_I(F) = +^1/_2$ and $-^1/_2$ are shifted away from the center of the spectrum.

A final complication in the interpretation of this spectrum is that there are several extra lines present which cannot be explained in the conventional analysis assuming axial symmetry. Similar features were observed in spectra of CF_3· which were explained[9,10] by the fact that, while the hyperfine tensors of each of the fluorine atoms are equivalent, they are not mutually parallel. This causes the axial component of the tensor to be at an angle of 18° with respect to the C_{3v} symmetry axis.[9] As a result, singularities in the spectrum appear which correspond to orientations of the radical with respect to the applied field which are other than parallel or perpendicular.

In the spectrum of CF_3·, there are sets of lines which correspond to either the parallel or the perpendicular orientation. However, these do not occur in the positions expected from the values of the hfs. Because $a_F(\parallel) > a_F(\perp)$, the lines $|M_I(F)| = {}^3/_2$ which correspond to parallel alignment are shifted closer to the center of the spectrum, while those of

$|M_I(F)| = {}^1/_2$ are shifted away from the center. Shifts in opposite directions occur for the lines which correspond to the perpendicular orientation. The effective value, $a_F(||)$, is then given by eq 3, where $a_x = a_y$ and a_z are the principal values of the hyperfine tensor.

$$a_F^2(||) = a_z^2 \cos^2 \alpha + a_x^2 \sin^2 \alpha \quad (3)$$

The spectrum of $NF_3^+\cdot$ is more complicated because of the added anisotropy of the ^{14}N hfs. Here the nitrogen hyperfine tensor will determine the positions of the singularities of the spectrum. As a result, the treatment given by Maruani et al.[9,10] for $CF_3\cdot$ needs to be modified. We report here, effective values for the hyperfine tensor, determined from the extrema of the spectra. In units of mT, $a_F(||) = 30.8$, $a_F(\perp) = 3.3$, $a_N(||) = 11.49$, and $a_N(\perp) = 7.8$. In contrast, Mishra et al.[4] report $a_F(||) = 30.0$, $a_F(\perp) = 10.0$, $a_N(||) = 11.5$, and $a_N(\perp) = 9.0$. The stick plot representing this analysis is shown in Figure 1b,c for the parallel and perpendicular orientations, respectively. The analysis of the parallel orientation is in agreement with the previous[4] assignment; however, there is substantial difference between our analysis of the perpendicular orientation and the previous one,[4] shown in Figure 1d. The analysis of the perpendicular components depends upon which features are selected. Since these features are buried within the spectrum and since extra lines appear, this assignment is indeed difficult. However, because of the large value of $a_F(||)$, there are downfield shifts of 1–5 mT due to second-order effects. Therefore, the features corresponding to the perpendicular orientation are those which are asymmetric with respect to the center of the spectrum, after allowing for the second-order splittings of the $|M_I(F)| = {}^1/_2$ lines. Furthermore, the features that we have selected are consistent with the analyses of high-temperature spectra as well as those derived from the $^{15}NF_3^+\cdot$ spectra.

Low-Temperature Spectra of $^{15}NF_3^+$. In order to confirm the analysis of the $^{14}NF_3^+\cdot$ spectra, samples of isotopically pure $^{15}NF_4^+$ salts were prepared. Since only 15 mg of sample was available, long irradiation times were used to get a sufficiently strong signal. This resulted in some line broadening. Nevertheless, because the spectra are less complicated, some features of the $\perp$ orientation can be observed. The result of the analysis is given in Table I. Within experimental error, the fluorine hfs are equivalent for $^{14}NF_3^+\cdot$ and $^{15}NF_3^+\cdot$, while their nitrogen hfs are in the ratio of their nuclear magnetogyric ratios (−1.403). The observed spectrum and a stick-plot of the analysis are shown in Figure 2. Note also that the spectrum exhibits anomalies similar to those discussed for $^{14}NF_3^+\cdot$.

High-Temperature Spectra of $^{14}NF_3^+\cdot$. The high-temperature spectrum of $^{14}NF_3^+\cdot$ shown in Figure 3 can be interpreted in terms of an axially symmetric radical containing three nuclei of $I = {}^1/_2$ and one nucleus of $I = 1$. A unique feature of this spectrum is that the hfs for the parallel orientation are smaller than those of the $\perp$ orientation. However, as discussed earlier, the features representing the $\perp$ orientation are considerably stronger than those of the $||$ orientation. As a result, the features of the parallel orientation in the middle of the spectra are masked, and they can only be determined by computer simulation. For $^{14}NF_3^+\cdot$ in NF_4AsF_6, the spectrum is interpreted in terms of a nitrogen nucleus ($I = 1$) and three equivalent fluorine nuclei ($I = {}^1/_2$). The hyperfine splittings are, in mT, $a_N(\perp) = 9.36$, $a_N(||) = 8.70$, $a_F(\perp) = 12.48$, and $a_F(||) = 2.00$. These values are independent of temperature between 235 and 340 K.

High-Temperature Spectra of $^{15}NF_3^+\cdot$. In order to confirm the assignment of the $^{14}NF_3^+\cdot$ spectra, spectra of a γ-irradiated sample of $^{15}NF_4AsF_6$ were obtained (Figure 4). These spectra can be analyzed in terms of one ^{15}N atom ($I = {}^1/_2$) and three equivalent ^{19}F atoms ($I = {}^1/_2$). The hyperfine splittings are given in Table I. The $^{15}NF_3^+\cdot$-containing samples exhibited the same thermal stability as the $^{14}NF_3^+\cdot$-containing samples described above.

Comparison of High- and Low-Temperature Spectra. The g factors and hyperfine splittings of the different $NF_3^+\cdot$ ESR spectra are given in Table I. That they are all due to $NF_3^+\cdot$ is established by the following observations: spectra of the irradiated ^{14}N and ^{15}N salts contain nuclei of the correct spins and numbers; fluorine atom hfs of $^{14}NF_3^+\cdot$ and $^{15}NF_3^+\cdot$ are equal at high and low temperatures, respectively, while the respective N-atom hfs are in the correct ratio of their nuclear moments; high-temperature spectra reversibly change into the low-temperature spectra, which are less intense; computed values of the isotropic hfs are the same in high- and low-temperature spectra, provided that the sign of $a_F(\perp)$ at low temperature is taken as negative.

The reason for the difference between the high-temperature and the low-temperature spectra is probably due to temperature-dependent rotation of $NF_3^+\cdot$ about a single axis. Spectra of $CF_3\cdot$ in a 1:30 CF_3I/Kr matrix change from one characteristic of a stationary radical to one characteristic of a freely rotating radical, as the temperature is increased from 4.2 to 35 K.[10] Examples in which similar changes occur between 77 and 300 K include $NH_3^+\cdot$ and $ND_3^+\cdot$ in their respective ammonium perchlorates[22] and $PF_5^-\cdot$ in KPF_6.[23,24] The averaging processes for $NH_3^+\cdot$ and $ND_3^+\cdot$,[22] as well as $PF_5^-\cdot$,[24] were attributed to rotations of these radical ions.

As the temperature of the $NF_3^+\cdot$-containing samples is increased, the spectra change between two different anisotropies. At low temperatures, the spectra are indicative of motionless $NF_3^+\cdot$, while at high temperatures, the spectra are indicative of uniaxial rotation. Most likely, this rotation occurs about an axis close to that of its minimum moment of inertia and is probably accompanied by some libration. Preliminary X-ray studies[26] on NF_4BF_4 show that the lattice is tetragonal, which may provide a preferential direction for rotation of the smaller $NF_3^+\cdot$ cation. Since this radical should be in its minimum energy configuration, significant deviations from the energetically favored pyramidal structure are extremely unlikely. Also, there are no phase changes of the lattice between 100 K and room temperature as indicated by Raman spectroscopy.[25] Inversion of the radical about the nitrogen would be expected to result in more nearly complete averaging.

Supporting evidence for rotation of $NF_3^+\cdot$ is provided by the fact that the $a_F(\perp)$ values observed for $^{14}NF_3^+\cdot$ and $^{15}NF_3^+\cdot$ are not identical. Since $NF_3^+\cdot$ has a pyramidal structure (see below), the moments of inertia of $^{14}NF_3^+\cdot$ and $^{15}NF_3^+\cdot$ must be different. This causes their rotational axes to be different, resulting in different $a_F(\perp)$ values.

UV-photolyzed mixtures of NF_3, BF_3, and Lewis acid at low temperatures exhibited spectra which were similar to that of Figure 1, except that the lines were broader. The line width increased slightly with longer photolysis, while the intensity increased. The higher temperature spectra (see for example Figure 5) can be interpreted in terms of the hyperfine parameters of the $NF_3^+\cdot$ spectra observed for the γ-irradiated salts (see Figure 3), although the line widths are quite different. For the photolyzed samples, the transition between the low and higher temperature spectra occurred at much lower temperatures than the γ-irradiated salts and the thermal stability of the radical depended upon the volatility of the Lewis acid used (see Results section). This suggests that these radicals are associated with solid AsF_5 or BF_3. The weaker residual signals observed after complete evaporation of the NF_3–F_2–Lewis acid condensed phases are similar to those in the γ-irradiated $NF_4^+\cdot$ salts. This suggests that they are due to $NF_3^+\cdot$ trapped in small amounts of $NF_4^+\cdot$ salts formed during the photolysis.

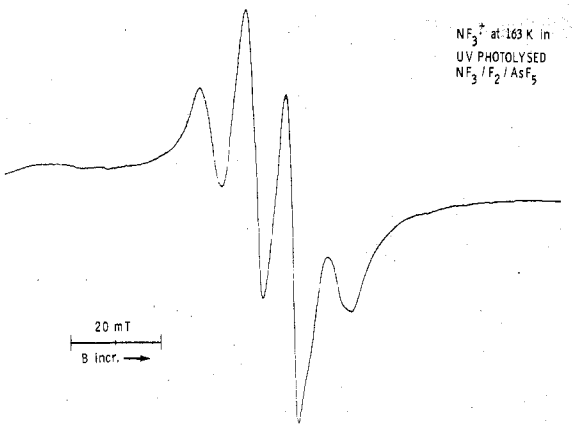

Figure 5. ESR spectrum of the $NF_3^{+}\cdot$ radial at 163 K produced by UV photolysis of a mixture of NF_3–F_2–AsF_5 (1:4:1) at 77 K. Comparison with Figure 1a shows that the six intense lines of the spectra are broadened into four overlapping lines, with the wings not resolved.

Table II. Comparison of Hyperfine Couplings of Radicals XF_3 Used in Table III

	$^{14}NF_3^{+}\cdot$,[a]	$^{12}CF_3\cdot$ and $^{13}CF_3\cdot$	$^{11}BF_3^{-}\cdot$,[b]	$^{14}NF_2O\cdot$,[c]
$a_X(\perp)$	7.8[d]	24.7[f]		
$a_X(\parallel)$	11.49[d]	31.8[f]		
$a_F(\perp)$	(−)3.3[d]	8.4[g]		
$a_F(\parallel)$	30.8[d]	26.4[g]		
a_F(iso)	8.98[e]	14.25[h]	17.8	14.34
a_X(iso)	9.14[e]	27.15[h]	15.3	9.39
g(iso)	2.0051[e]	2.0031[h]	2.0021	2.0058

[a] This work. [b] Reference 5. [c] References 27 and 28. [d] Taken from low-temperature spectra. [e] Taken from high-temperature spectra. [f] Reference 29. [g] Reference 9. [h] Reference 6.

Table III. Spin Densities on the Central Atom and Fluorine Atoms of $NF^{+}\cdot$ Compared to Those of Related Radicals

radical	$\rho_X^s(X)$	$\rho_X^p(X)$	ρ_F^s	g(iso)
$BF_3^{-}\cdot$	0.212		0.0104	2.0021
$CF_3\cdot$	0.245	0.717	0.0084	2.0029
$NF_3^{+}\cdot$	0.166	0.687	0.0053	2.0051
$NF_2O\cdot$	0.170		0.0084	2.0058
$NF_2\cdot$	0.030	0.956	0.0052	2.0044

[a] Spin densities calculated from the data in Table II, assuming that atomic isotropic hyperfine couplings a° in mT are 72.1 for B, 111.0 for C, 55.0 for N, and 17100 for F, and the atomic anisotropic couplings b° are 3.24 for C and 1.71 for N. (See ref 30.)

Structures of $NF_3^{+}\cdot$. ESR data for $NF_3^{+}\cdot$ and isoelectronic species are compared in Table II. Since the tensors of the fluorine hfs need not be exactly axially symmetric, we averaged those in the $CF_3\cdot$ radical[9] to yield an effective value to be compared with that of $NF_3^{+}\cdot$. The spin densities on the s and p orbitals, ρ_i^s and ρ_i^p, respectively, of the central atom, given in Table III, were calculated by eq 4 and 5, where a_i and b_i

$$\rho_i^s = a_i(\text{iso})/a_i^\circ \quad (4)$$

$$\rho_i^p = (a_i(\parallel) - a_i(\text{iso}))/2b_i^\circ \quad (5)$$

are the isotropic and anisotropic hfs of an electron in the s and p orbitals of atom i, and a_i(iso) is the calculated isotropic hfs. For $BF_3^{-}\cdot$, no experimental anisotropic hfs were available, and values calculated from ref 31 had to be used.

The values of ρ_N^s for $NF_3^{+}\cdot$ and $NF_2O\cdot$ are nearly the same, as expected from the isoelectronic character of the -F: and -O: substituents. Although the ρ^s values for the series $NF_3^{+}\cdot$, $CF_3\cdot$, and $BF_3^{-}\cdot$ do not follow a monotonic trend, without a measured value for the anistropic boron hfs, the hybridization cannot be accurately determined. The value of ρ^p/ρ^s for $CF_3\cdot$ is 2.9, while that of $NF_3^{+}\cdot$ is 4.1. This suggests that the free electron in $NF_3^{+}\cdot$ has more p character than that in $CF_3\cdot$. This in turn suggests that the hybridization of the XF bonds in $CF_3\cdot$ is nearly sp^3 but that in $NF_3^{+}\cdot$ is between sp^3 and sp^2. This in turn indicates that $NF_3^{+}\cdot$ is more planar than $CF_3\cdot$ in contrast to the conclusion of Mishra et al.[4] This is further supported by the fact that the observed anisotropy in the fluorine hfs is greater for $NF_3^{+}\cdot$ than for $CF_3\cdot$. Recent theoretical calculations[31] based on the isotropic hfs of $BF_3^{-}\cdot$, $CF_3\cdot$, and $NF_3^{+}\cdot$ also indicate that the planarity increases from $BF_3^{-}\cdot$ toward $NF_3^{+}\cdot$.

The same conclusions are reached if the values of a_i° and b_i° reported by Hurd and Coodin[32] are used. These values are approximately 15% larger than those used here, so that smaller spin densities are computed. Although these absolute values appear more realistic, they leave the ratios of ρ^p/ρ^s unchanged.

The spin densities of $NF_3^{+}\cdot$ and $NF_2\cdot$ are also compared in Table III. The spin density distribution for $NF_2\cdot$ is calculated from the ESR data of Kasai and Whipple,[33] and the data are consistent with the isotropic data of Farmer et al.[35] Values in mT are $a_N(\parallel) = 4.9$, $a_N(\perp) = 0.0$, $a_F(\parallel) = 21.2$, and $a_F(\perp) = -16.9$. In $NF_2\cdot$, the unpaired electron is primarily in a p orbital so that there is no delocalization of the unpaired electron into the orbital of the lone pair on nitrogen. Thus, the structure of this radical is surprisingly different from that of $NF_3^{+}\cdot$.

Work is underway to analyze, in detail, the hyperfine splittings of the $NF_3^{+}\cdot$ radical and determine the angle α between the nitrogen and fluorine hyperfine tensors. In the $CF_3\cdot$ radical, α was found to be 17.8°.[9,10] Edlund et al.[35] reported that the direction of the hfs was not perpendicular to the C–F bond, but at an angle of 54° to it. A precise analysis of the low-temperature spectrum of $NF_3^{+}\cdot$ may substantiate the above conclusions. Since the $NF_3^{+}\cdot$ radical is slightly more planar, α for $NF_3^{+}\cdot$ may be different from that of $CF_3\cdot$.

Acknowledgment. This work was supported in part by the U.S. Army Research Office and the Office of Naval Research. We thank John Coope (University of British Columbia) Ffrancon Williams (University of Tennessee), Martyn Symons (University of Leicester), and L. R. Grant for helpful discussions, R. D. Wilson for experimental assistance, and O. Buck and D. Sellman for assistance with the γ-irradiation facility. We also thank L. K. White and R. L. Belford (University of Illinois) and N. D. Chasteen (University of New Hampshsire) for making their simulation programs available to us.

Registry No. $^{14}NF_3^{+}\cdot$, 37366-70-4; $^{15}NF_3^{+}\cdot$, 67745-75-9.

References and Notes

(1) P. W. Atkins and M. C. R. Symons, "The Structure of Inorganic Radicals", Elsevier, Amsterdam, 1967
(2) See, for example, I. B. Goldberg, K. O. Christe, and R. D. Wilson, *Inorg. Chem.*, **14**, 152 (1975).
(3) K. O. Christe and I. B. Goldberg, *Inorg. Chem.*, **17**, 759 (1978).
(4) S. P. Mishra, M. C. R. Symons, K. O. Christe, R. D. Wilson, and R. I. Wagner, *Inorg. Chem.*, **14**, 1103 (1975).
(5) R. L. Hudson and F. Williams, *J. Chem. Phys.*, **65**, 3381 (1976).
(6) R. W. Fessenden, *J. Magn. Reson.*, **1**, 277 (1969).
(7) R. W. Fessenden and R. H. Schuler, *J. Chem. Phys.*, **43**, 2704 (1965).
(8) M. T. Rogers and L. D. Kispert, *J. Chem. Phys.*, **46**, 3193 (1967).
(9) J. Maruani, J. A. R. Coope, and C. A. McDowell, *Mol. Phys.*, **18**, 165 (1970).
(10) J. Maruani, C. A. McDowell, H. Nakajima, and P. Raghunathan, *Mol. Phys.*, **14**, 349 (1968).
(11) W. Maya, *Inorg. Chem.*, **3**, 1063 (1964).
(12) K. O. Christe, C. J. Schack, and R. D. Wilson, *Inorg. Chem.*, **15**, 1275 (1976).
(13) K. O. Christe, C. J. Schack, and R. D. Wilson, *J. Fluorine Chem.*, **8**, 541 (1976).
(14) I. B. Goldberg, H. R. Crowe, and R. S. Carpenter II, *J. Magn. Reson.*, **18**, 84 (1975).

(15) G. K. Miner, T. P. Graham, and G. T. Johnston, *Rev. Sci. Instrum.*, **43**, 1297 (1972)
(16) I. B. Goldberg, unpublished research.
(17) J. R. Pilbrow and M. E. Winfield, *Mol. Phys.*, **25**, 1073 (1973).
(18) N. D. Chasteen, personal communication.
(19) P. C. Taylor and P. J. Bray, *J. Magn. Reson.*, **2**, 305 (1970).
(20) J.-L. Marill and D. Cornet, *J. Chim. Phys. Phys.-Chim. Biol.*, **70**, 336 (1973).
(21) N. M. Atherton, "Electron Spin Resonance", Hilger and Watts, London, 1973.
(22) K. V. S. Rao and M. C. R. Symons, *J. Chem. Soc. A*, 2163 (1971).
(23) P. W. Atkins and M. C. R. Symons, *J. Chem. Soc.*, 4363 (1964).
(24) S. P. Mishra and M. C. R. Symons, *J. Chem. Soc., Chem. Commun.*, 279 (1974).
(25) K. O. Christe, unpublished research.
(26) D. Lind, personal communication.
(27) K. Nishikida and F. Williams, *J. Am. Chem. Soc.*, **97**, 7166 (1975).
(28) N. Vanderkooi, J. S. MacKenzie, and W. B. Fox, *J. Fluorine Chem.*, **7**, 415 (1976).
(29) M. T. Rogers and L. D. Kispert, *J. Chem. Phys.*, **46**, 3193 (1967).
(30) J. E. Wertz and J. R. Bolton, "Electron Spin Resonance: Elementary Theory and Practical Applications", McGraw-Hill, New York, N.Y., 1972.
(31) S. P. So, *J. Chem. Phys.*, **67**, 2929 (1977).
(32) C. M. Hurd and P. Coodin, *J. Phys. Chem. Solids*, **28** 523 (1966).
(33) P. H. Kasai and E. B. Whipple, *Mol. Phys.*, **9**, 497 (1965).
(34) J. B. Farmer, M. C. L. Gerry, and C. A. McDowell, *Mol. Phys.*, **8**, 253 (1964).
(35) O. Edlund, A. Lund, M. Shiotani, J. Sohma, and K. A. Thuomas, *Mol. Phys.*, **32**, 49 (1976).
(36) K. O. Christe, R. D. Wilson, and C. J. Schack, *Inorg. Chem.*, **16**, 937 (1977).
(37) W. E. Tolberg, R. T. Rewick, R. S. Stringham, and M. E. Hill, *Inorg. Chem.*, **6**, 1156 (1967).

Contribution from Cattedra di Chimica Generale della Facoltà di Farmacia, the Istituto di Chimica Generale, and the Laboratorio CNR, Florence, Italy

Single-Crystal ESR Spectra of Copper(II) Complexes with Geometries Intermediate between a Square Pyramid and a Trigonal Bipyramid

ALESSANDRO BENCINI,[1a] IVANO BERTINI,*[1b] DANTE GATTESCHI,[1c] and ANDREA SCOZZAFAVA[1b]

Received March 30, 1978

The single-crystal ESR spectra of copper(II)-doped bis(*N*-methylsalicylaldiminato)zinc(II) and (bis(3-salicylaldiminatopropyl)methylamine)zinc(II) have been recorded. Both the complexes are five-coordinate with geometries intermediate between a square pyramid and a trigonal bipyramid. The g and A values of these complexes are discussed on the basis of an angular overlap model. Criteria are suggested for recognizing the ESR spectra of distorted five-coordinate complexes in diluted powders or frozen solutions.

Introduction

The ESR spectra of five-coordinate copper(II) complexes are now reasonably well understood as far as the two limiting square-pyramidal and trigonal-bipyramidal forms are concerned. The two forms can be easily recognized from the ESR spectra, since $g_\perp > g_\parallel \simeq 2.00$ and $|A_\parallel| \simeq |A_\perp| \simeq (60\text{–}100) \times 10^{-4}$ cm^{-1} for trigonal and $g_\parallel > g_\perp$ and $|A_\perp| \ll |A_\parallel| \simeq (120\text{–}150) \times 10^{-4}$ cm^{-1} for square-pyramidal complexes.[2-8] Also some magnetically undiluted complexes with intermediate geometries have been studied,[9-11] but no information is available on the values of the hyperfine coupling constants. Since five-coordinate complexes most commonly have geometries intermediate between the two limiting geometries,[12] is appeared interesting to us to study some model complexes in order to appreciate the pattern of variation of the spin-Hamiltonian parameters in passing from a pyramid to a bipyramid. We wish to report now the single-crystal ESR spectra of copper(II)-doped bis(*N*-methylsalicylaldiminato)zinc(II) (hereafter (Cu,Zn)SalMe)[13] and (bis(3-salicylaldiminatopropyl)methylamine)zinc(II) (hereafter (Cu,Zn)SalMeDPT)[14] (see the ligand structures below) and to compare the g and A values with a simple theoretical model which allows for the geometrical distortions from the idealized symmetry.

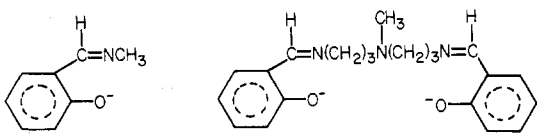

Experimental Section

All the compounds were prepared as previously described.[13,14] Single crystals of the copper doped into ZnSalMe and ZnSalMeDPT were obtained by slow evaporation of chloroform–benzene solutions. ZnSalMe crystallizes in the triclinic system: space group $P\bar{1}$; a = 9.48 Å, b = 10.53 Å, c = 8.45 Å, α = 99° 45′, β = 92° 58′, γ = 117° 58′; Z = 2.[15] The doped crystals were light green prisms with the (100) face most developed. ZnSalMeDPT crystals are monoclinic: space group $P2_1/c$; a = 6.913 Å, b = 13.975 Å, c = 19.893 Å, β = 91° 54′; Z = 4.[16] They were plates with the (001) face most prominent. Both types of crystals were oriented by Weissenberg techniques. The crystals were mounted on a Perspex cube, fitted to a Perspex rod. The morphological properties of the crystals were used to align them under a microscope. In the case of the monoclinic crystal the orientation was checked by the coincidence of the ESR signals of the two magnetically nonequivalent molecules in some particular orientation in the magnetic field. The ESR spectra were obtained using a Varian E-9 spectrometer equipped with X band. Three independent rotations along the three axes of the Perspex cube were performed. All of the spectra were recorded at liquid nitrogen temperature.

Results

(Cu,Zn)SalMe. The complex ZnSalMe is dimeric, formed by two trigonal-bipyramidal moieties sharing one axial and one equatorial ligand[15] (Figure 1). CuSalMe has a different coordination polyhedron but it assumes the same coordination as the zinc analogue when doped into the lattice of the latter compound.[17] Diluted solid solutions have been used in order to ensure that the coupling between the copper atoms is negligible; indeed no signal was observed in the spectra which could be attributed to directly interacting couples of copper atoms. The Z laboratory axis corresponds to the {010} direction whereas the X axis lies in the (010) plane making an angle of 9° 45′ with the $+c$ axis. In the rotation along the Y laboratory axis an extreme g value of 2.25 is found, which closely corresponds to the highest g value of the powder spectra (Figure 2). Also the value of the hyperfine coupling constant coincides with that of the powder spectra. The principal g values have been determined through the Ayscough method[18] and are shown in Table I, together with the coordinates of the points which identify the g_1, g_2, and g_3 directions in the triclinic unit cell. The g_2 and g_3 extremes were checked also by rotating around an axis parallel to the g_1 direction. The directions of

0020-1669/78/1317-3194$01.00/0